Structural Basis of the Anionic Interface Preference and k^*_{cat} Activation of Pancreatic Phospholipase A_2[†]

Bao-Zhu Yu,[‡] Ming Jye Poi,[§] U. A. Ramagopal,[#] Rinku Jain,[#] S. Ramakumar,[#] Otto G. Berg,*[,⊥] Ming-Daw Tsai,*[,§] K. Sekar,*[,#] and Mahendra Kumar Jain*[,‡]

Department of Chemistry and Biochemistry, University of Delaware, Newark, Delaware 19716, Department of Physics and Bioinformatics Centre, Indian Institute of Science, Bangalore, India, Departments of Chemistry and Biochemistry and Ohio State Biochemistry Program, The Ohio State University, Columbus, Ohio 43210, and Department of Molecular Evolution, Uppsala University Evolutionary Biology Center, Uppsala, Sweden

Received March 31, 2000; Revised Manuscript Received July 24, 2000

ABSTRACT: Pancreatic phospholipase A_2 (PLA2) shows a strong preference for the binding to the anionic interface and a consequent allosteric k^*_{cat} activation. In this paper, we show that virtually all the preference is mediated through 3 (Lys-53, -56, and -120) of the 12 cationic residues of bovine pancreatic PLA2. The lysine-to-methionine substitution enhances the binding of the enzyme to the zwitterionic interface, and k^*_{cat} for the K53,56,120M triple mutant at the zwitterionic interface is comparable to that for the wild type (WT) at the anionic interface. In the isomorphous crystal structure, the backbone folding of K53,56M K120,121A and WT are virtually identical, yet a significant change in the side chains of certain residues, away from the site of substitution, mostly at the putative contact site with the interface (i-face), is discernible. Such reciprocity, also supported by the spectroscopic results for the free and bound forms of the enzyme, is expected because a distal structural change that perturbs the interfacial binding could also affect the i-face. The results show that lysine-to-methionine substitution induces a structural change that promotes the binding of PLA2 to the interface as well as the substrate binding to the enzyme at the interface. The kinetic results are consistent with a model in which the interfacial Michaelis complex exists in two forms, and the complex that undergoes the chemical step is formed by the charge compensation of Lys-53 and -56. Analysis of the incremental changes in the kinetic parameters shows that the charge compensation of Lys-53 and -56 contributes to the k^*_{cat} activation and that of Lys-120 contributes only to the structural change that promotes the stability of the Michaelis complex at the interface. The charge compensation effects on these three residues also account for the differences in the anionic interface preference of the evolutionarily divergent secreted PLA2.

Regulation of the interfacial catalytic behavior of an enzyme by the interface is not adequately understood, and the structural basis for the interface preference is one of the major unresolved problems in interfacial enzymology. For a general formulation of the consequences of interfacial catalysis and activation, we have characterized the catalytic behavior of pancreatic phospholipase A_2 (PLA2)[1] in terms of the primary interfacial rate and equilibrium parameters (*1*−*10*). Significantly higher rates of hydrolysis of PLA2 at anionic interfaces, relative to those at zwitterionic interfaces, have been dissected into enhanced binding of PLA2 (*4*, *6*, *7)* and the allosteric k^*_{cat} activation for the turnover at the interface (*6*, *8*, *9*). Such a preference for the anionic interface, attributed to a change in the intrinsic properties of the enzyme at the interface, is clearly discernible from the apparent rate enhancement due to an increased substrate replenishment in the microenvironment of the enzyme at the interface (*10*−*13*).

Having resolved the functional consequences of the anionic interface preference in terms of the primary parameters, in this paper we identify the cationic residues that contribute to the anionic interface preference of bovine pancreatic PLA2. Since the natural substrate of pancreatic PLA2 is codispersed with anionic bile salts, a role for cationic residues has been widely recognized (*9*, *14*−*20*). The anionic interface preference is a general property shared to varying degrees by several evolutionarily divergent secreted PLA2 isoforms and other interfacial enzymes. Our earlier analysis of the kinetic effects of the single lysine substitutions (*9*) and deletions (*20*) in bovine PLA2 had suggested an incremental role for Lys-53, -56, -120, and -121 in the anionic interface

[†] This work was supported by PHS (GM29703 to M.K.J., GM41788 to M.D.T.), Swedish NSRC (O.G.B.).

* To whom correspondence should be sent. Phone: 302-831-2968; fax: 302-831-6335; e-mail: mkjain@udel.edu.

[‡] University of Delaware.

[§] Ohio State University.

[#] Indian Institute of Science.

[⊥] Uppsala University.

[1] Abbreviations: CMC, critical micelle concentration; DC_7PC, 1,2-diheptanoylglycero-*sn*-3-phosphocholine; deoxy-LPC, 1-hexadecylpropanediol-3-phosphocholine; DMPC, dimyristoyl-*sn*-3-glycerophosphocholine; DOPC, dioleoyl-*sn*-3-glycerophosphocholine; i-face, the interfacial contact face of PLA2; MJ33, 1-hexadecyl-3-(trifluoroethyl)-*rac*-glycero-2-phosphomethanol; PLA2, phospholipase A_2 from bovine pancreas (nmPLA2, isozymes from *Naja melanoleuca* venom; app-PLA2, the monomer isozyme from *Agkistrodon piscovorus piscovorus* venom); WT, bovine pancreatic PLA2.

10.1021/bi000740k CCC: $19.00
Published on Web 09/08/2000

preference. The fact that these residues are in two well-separated regions of PLA2 is particularly suggestive because the interface-binding controls k^*_{cat} (*9*).

Building on these leads, results in this paper show that the anionic interface preference of WT bovine pancreatic PLA2 is substantially, if not entirely, due to the charge compensation of Lys-53, -56, and -120 and a consequent structural change in the substitution mutant. For example, the K53,56,120M triple mutant has a higher (30×) affinity for the zwitterionic interface with a 15-fold higher k^*_{cat} relative to the WT. The two sequential state model shown below is a useful guide for the experimental design and interpretation of results.

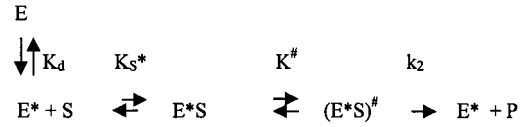

Thus, the enzyme in the aqueous phase (E) binds to the interface as a prelude to the catalytic turnover at the interface through the species marked with an asterisk (E*, E*S). Note that calcium is an obligatory cofactor for the substrate binding and the chemical step; however, for clarity we have only implicitly included calcium in this scheme or in the discussion. In this minimal modification to our standard kinetic scheme for interfacial enzymology (*1*−*6*), the ternary Michaelis complex exists in two forms with $K^{\#} = [E^*S]/[E^*S]^{\#}$. Only $(E^*S)^{\#}$ undergoes the chemical change. Thus E*S predominates in WT at the zwitterionic interface, and it is converted to the activated $(E^*S)^{\#}$ form at the anionic interface or by added NaCl or by the lysine-to-methionine substitutions. Since the anionic interface preference is a general property of several interfacial enzymes, broad kinetic, structural, regulatory, and evolutionary significance of this phenomenon are discussed.

EXPERIMENTAL PROCEDURES

Sources of reagents and protocols (kinetic, spectroscopic, crystallographic, analytical, and structural) have been described before (*1*−*14*, *20*−*27*). Only salient details are outlined below. Some of the results from earlier publications are included in this paper for comparison purposes. DC_7PC, DMPC, and DOPC were from Avanti Polar Lipids. All other reagents were analytical grade. Uncertainty in measured values is 10% and that in the derived parameters is 30%.

Site-Directed Mutagenesis and Protein Purification. Construction, X-ray structure, including preliminary kinetic results with single K53 and K56 substitution mutants of PLA2, have been described (*14*, *20*−*24*). The same protocols were adopted for the construction and characterization of the additional mutants listed in Table 2. Mutants were generated with oligonucleotides in complementary sets: 5′ CACAAGAATCTTGATATGAAAAACTGT TAAGCTT 3′ (K120 to M); 5′ AACACAAGAATCTTGATATGAT-GAACTGTTAAG CTTCTG 3′ (K120, K121 to M); 5′ TGCTATAAACAAGCTATGAAACTTGATAGCT GC 3′ (K56 to M); 5′ CATGATAATTGCTATATGCA AGCTAAA-AAACTT 3′ (K53 to M); 5′ CAAGAATCTTGATAAAAT-GAACTGTTAAGCTTCT 3′ (K121 to M).

In all cases, the Quickchange method (Stratagene) with ET25b(m)-proPLA2 template was used. Double, triple, and quadruple mutants were generated by using their corespondent single, double, and triple mutant pET25b(m)-proPLA2 as templates. The recombinant PLA2 mutants were expressed in *Escherichia coli* BL 21 (DE3) pLys S (Novagen) strain as inclusion-body protein, which was refolded (*24*).

Kinetic Protocols. Unless indicated, all kinetic measurements were carried out in 0.5 mM $CaCl_2$ for the hydrolysis of DMPM and 10 mM $CaCl_2$ for DC_7PC at 25 °C and pH 8.0 in a nitrogen-purged atmosphere by the pH-stat method using 3 mM NaOH titrant on a Brinkman (Metrohm) or a Radiometer titrator with a strip chart recorder (*1*, *6*). Stock dispersions of DC_7PC or other lipids in water were added to the reaction mixture and equilibrated. Necessary corrections were made for the background pH drift in the absence of the enzyme. The reaction was initiated by the addition of 0.1−30 pmol of PLA2 depending on the observed rate. Hydrolysis commenced in less than 3 s after the addition of enzyme. The observed rate varied linearly with the amount of enzyme. Inhibitor and other components, if present in the reaction mixture, were added before or after initiating the reaction. Results in the presence of 4 M NaCl have been corrected for a small change in the titration efficiency determined by adding a known amount of myristic acid or heptanoic acid to the reaction mixture in the absence of PLA2. Controls showed that the sequence of addition of the substrate or PLA2 does not noticeably affect the apparent parameters, K_M^{app} and V_M^{app} (*7*). Initial rates and all the rate parameters are expressed as turnover number per second.

X-ray Crystallography of K53,56M PLA2. Crystals that could diffract to 1.9-Å resolution were obtained at room temperature (293 K) using the hanging drop vapor diffusion method. The crystals grew over a period of 2−3 weeks. The crystallization droplet contained 5 μL of protein solution [15 mg/mL in 50 mM Tris buffer, pH 7.2, and 2 μL of 60% 3-methyl-2,4-pentanediol (MPD)]. The reservoir contained 50% MPD. The crystal was trigonal, space group $P3_121$ with the unit cell parameters $a = b = 46.41$ Å and $c = 102.72$ Å. For comparison with the WT, we used the structure (PDB 1MKT) from the isomorphous trigonal crystals (*28*).

Complete X-ray intensity data were collected from a single crystal with dimensions 0.25 × 0.25 × 0.40 mm at room temperature using a 300-mm Mar Research imaging plate detector mounted on a Rigaku rotating anode generator equipped with a CuKα target operated at 40 kV and 58 mA. The data were processed up to 1.9-Å resolution with DENZO suite of packages (*29*, *30*). A total of 42 068 observations were collected which gave 9733 unique reflections with a R_{merge} of 9.2%.

The atomic coordinates of the trigonal form of the WT PLA2 (PDB 1MKT) were used as the starting model (*28*). A total of 949 reflections (10%) were used to calculate the R_{free} (*31*) to monitor the progress of the refinement. Initially 30 cycles of rigid body refinement were carried out, followed by 50 cycles of positional refinement by Powell energy minimization. Without the mutated residues, Met-53 and Met-56, the *R*-value was 28.5% [$R_{free} = 29.2\%$] for 8033 reflections in the resolution range 10−1.9 Å. The mutated methionine residues were then inserted and fitted into the electron density map. The model was subjected to simulated annealing by employing a slow-cooling protocol, starting from 3000 K and slowly cooling to 300 K in steps of 25 K

Table 1: Comparison of the Anomalous Kinetic Effects at the Zwitterionic Interfaces for PLA2 from Different Sources

PLA2 isoform (K or R changed in bovine PLA2[a])	anomalous effects		
	CMC	NaCl	delay
IB pancreas:			
bovine	yes	yes	yes
pig (12A, 57N)	yes	yes	yes
iso-pig (12T)	yes	yes	yes
horse (10Q,12T, 43A,53T,57E, 113P)	yes	yes	yes
sheep (108E,113N)	yes	yes	yes
IA venom nmDEI (10H, 53D, 56E, δ62−66, 120N)	yes	no	no
IIA human (10I,12I,43F,57D,108C,113A,115A,121N)	yes	yes	yes
IIB venom appPLA (53G, δ62−66,108D,113S,120P,121L)	yes	yes	yes
III bee venom PLA2 (not homologous)	yes	no	yes

[a] Sequence information (*35*, *43*). Bovine PLA2 has Arg or Lys at 10, 12, 43, 53, 56, 57, 62, 108, 113, 115, 120, 121.

at 0.5 fs, followed by 100 cycles of positional refinement to the *R*-value of 24.1% [R_{free} = 29.2%]. The resulting difference electron density maps clearly revealed the calcium ion. In addition, 65 water (oxygen atoms) were picked and included in the refinement. The 123 amino acid residues of the protein, the calcium ion, and the 65 water molecules were subjected to a few more cycles of positional and individual isotropic B-factor refinement. During the progress of the refinement, additional water molecules were picked and included. Omit maps (omitting 20 residues at a time) were calculated and used to correct or check the final protein model. The final *R*-value was 18.9% [R_{free} = 22.4%] with 106 water molecules included along with 955 non-hydrogen atoms of the protein and one calcium ion. The program X-PLOR 3.1 (*32*) was used for the refinement, and the program FRODO (*33*) was used for molecular modeling. The atomic coordinates for K53,56M are deposited in the PDB (*34*) as 1C74, with R1C74SF for the structure factors.

RESULTS

Anomalous Kinetic Effects for Pancreatic PLA2 at Zwitterionic Interfaces. Patterns of significant functional differences have been noted between the various types of evolutionarily divergent 14-kDa secreted PLA2 from venoms, pancreas, and inflammatory cells (*27*, *35*−*45*). In general, the anomalous kinetic effects observed at the zwitterionic interfaces are not seen at anionic interfaces. Such differences, in conjunction with the sequence differences of the evolutionarily divergent PLA2, provide an initial guide for the identification of the cationic residues that determine the anionic interface preference of bovine PLA2. Three criteria (Table 1) for the anomalous kinetics are useful: the rate enhancement above the critical micelle concentration of DC_7-PC (CMC effect), a rate enhancement on DC_7PC micelles with added NaCl, and a delay in the onset of the steady-state on DMPC vesicles. All types of secreted PLA2 show an enhanced rate of hydrolysis above the CMC. Such a CMC effect at zwitterionic micellar interface is an important criterion for interfacial catalysis because the enzyme must bind to preformed micelles for the catalytic turnover (*4*, *6*, *17*, *27*, *40*). In contrast, the rate of hydrolysis with the monodisperse DC_7PC is negligible, and well below most reported values, if the reaction on air bubbles and vessel walls is eliminated (*41*). Also nmPLA2 DE3 forms premicellar aggregates with monodisperse zwitterionic substrates, and therefore the observed rate does not show the CMC effect (*45*).

Rationale for the Substitution of the Cationic Residues that Control the Anionic Charge Preference. Operationally, we attribute the NaCl and the delay effects to the interfacial anionic charge preference because such effects are not observed at the anionic interfaces. The rate enhancement by added NaCl is due to a preferential partitioning of chloride anion in the zwitterionic interface (*6*). Similarly, the enhanced hydrolysis of zwitterionic DMPC vesicles after a delay is due to the anionic charge from the accumulated products of hydrolysis in the bilayer (*39*). Results in Table 1 show that all type of PLA2 show the CMC effect. Activation by added NaCl is not seen with type IA nmPLA2 or with type III beePLA2, and nmPLA2 is the only exception for the delay effect. We drop bee venom PLA2 from further consideration because its folded structure is significantly different than the other types of PLA2; however, the bee PLA2 results imply that the delay and the salt effects may have a different origin under certain conditions.

To identify the origin of the interfacial anionic charge preference, we compared the positions of the cationic residues found in IA nmPLA2 to those found in IB bovine and other PLA2 isoforms. The rationale is that only the cationic residues of interest are those present in all secreted PLA2 that show the charge preference, and the comparison also provides key criteria for eliminating the cationic residues that do not contribute toward the preference. A lack of the charge preference by the nmPLA2 provides a template for the evolutionary changes that led to the anionic interface preference. Bovine pancreatic PLA2 has 12 cationic residues. On the basis of results in Table 1, we discount the contribution of the cationic residues 10, 12, 43, 57,108, 113, 115, and 121 in mediating the anionic interface preference. For example, we discount a role for residues at 12 because IB pig PLA2 has Ala-12 and iso-PLA2 has Thr-12. Similarly, 57 is also eliminated on the basis of the pig PLA2 results.

With this pruning of the unlikely possibilities, the cationic residues in positions 53, 56, 62, and 120 are implicated in mediating the anionic charge preference of bovine PLA2. This assertion is consistent with the fact that the nmPLA2, which does not show the anionic interface preference, does not have cationic residues in positions 53, 56, 120, and the 62−66 loop is deleted. Note that the sequence alignment toward the C-terminus is somewhat speculative due to loop deletions (*27*, *35*, *42*, *43*). Our rationale for not considering the substitution of residue 62 is that the appPLA2 with the missing 62−66 loop does not exhibit the charge preference. Earlier studies also indicated that the charge preference of bovine PLA2 is partially modified by single substitutions of 53 and 56 (*9*, *44*). Collectively, these comparisons suggest a concurrent role for several cationic residues, possibly 53, 56, 120, and 121, in determining the anionic interface preference of these diverse types of secreted PLA2. We show below that the lysine-to-methionine substitution of 53, 56, and 120 eliminates the anionic interface preference of WT.

Kinetic Parameters for the Lysine Substitution Mutants. The dependence of the rate of hydrolysis by PLA2 on the

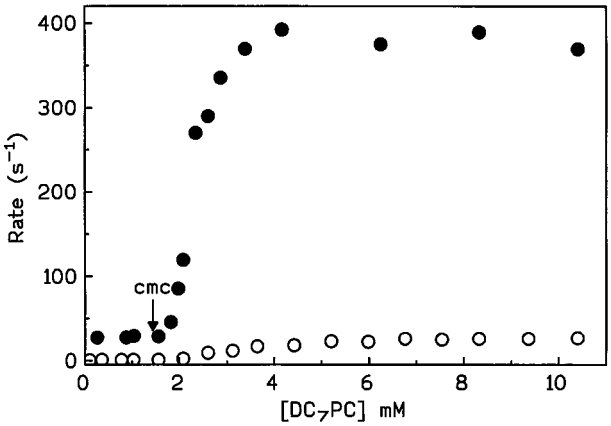

FIGURE 1: Effect of the bulk DC_7PC concentration on the initial rate of hydrolysis in 1 mM NaCl by bovine pancreatic PLA2 (open circle) WT and (filled circles) K53,56,120M mutant. Note that the rate of hydrolysis above the critical micelle concentration (cmc) is considerably enhanced for the mutant.

concentration of DC_7PC shows a dramatic increase above the critical micelle concentration (Figure 1). The plot of rate versus the micellar DC_7PC concentration shows a hyperbolic dependence from which we obtained the apparent parameters K_M^{app} and V_M^{app} (*6*) in the presence of 1 mM and 4 M NaCl for the substitution mutants (Table 2). The analytic basis and validity of the assumptions for the turnover in the pseudo-scooting conditions, under the limit of fast substrate and products exchange, has been demonstrated (*6*). Thus, the apparent parameters are related to K_d, K_M^*, and k_{cat}^* by eq 1−3. Here K_S' is the critical micelle concentration of the substrate, and K_M is the Michaelis constant for the ES form in the aqueous phase. The nomenclature and the significance of the parameters conform to classical enzymology with the proviso that the initial binding of the enzyme to the bulk interface is described by the dissociation constant K_d for E*. The maximum possible mole fraction of the substrate, $X_s = 1$. Also $X_I(50)$, K_I^*, and K_M^* values are in units of mole fraction, as related to the fraction of the molecules at interface that the bound enzyme "sees". The $X_I(50)$ (column 6 or 10 in Table 2) is the mole fraction of MJ33 in the interface for 50% inhibition of the initial rate at the saturating levels of the bulk substrate concentration. The K_I^* values for MJ33 (column 3) were independently determined by the protection method (*7*, *26*). Both of these parameters were used to calculate the interfacial K_M^* for DC_7PC (column 7 and 11, Table 2).

$$V_M^{app} = \frac{X_s k_{cat}^*}{X_S + K_M^*} \quad (1)$$

$$K_M^{app} = \frac{K_d K_M^*}{X_S + K_M^*}\left(1 + \frac{K_S}{K_M}\right) \quad (2)$$

$$\frac{1 - X_I(50)}{X_I(50)} = \left(\frac{1 + 1/K_I^*}{1 + 1/K_M^*}\right) \quad (3)$$

Results in Table 2 show that the most significant effect of the lysine substitutions is on V_M^{app} in 1 mM NaCl, i.e., the maximum rate at the saturating bulk DC_7PC concentration increases from about 30 s^{-1} for WT to 460 s^{-1} for the triple (#6) or quadruple (#10) mutant. On the other hand, V_M^{app} values in 4 M NaCl are in the 500 to 900 s^{-1} range. Typically, the activating effect of 4 M NaCl, relative to the rate in 1 mM NaCl, decreases with an increasing number of lysine substitutions. Also, the rank order for the incremental changes for single substitutions is 56 > 53 > 120 ≫ 121. V_M^{app} in 1 mM NaCl is maximum for the triple mutant K53,-56,120M (#6), and the fourth substitution (#10) does not significantly increase the rate in 1 mM NaCl. Note that a modest 2× salt effect is still seen with the triple mutant (#6) and a 1.5× effect with the quadruple mutant (#10). Such residual effects of the charge preferences suggest a modest role for a yet unidentified cationic residue. The origin and the magnitude of the incremental changes in the primary parameters that cause the changes in K_M^{app} and V_M^{app} are analyzed below.

Effect of Lysine Substitutions on the Substrate Binding and the Chemical Step. $X_I(50)$ for MJ33 (Table 2, columns 6 and 10) are marginally higher for the multiple substitution mutants. The K_I^* values (Table 2, column 3) suggest that the intrinsic affinity of PLA2 for the competitive inhibitor MJ33 increases significantly with the lysine substitutions. K_M^* (Table 2, column 7 and 11) was calculated on the basis of eq 3 from $X_I(50)$ and K_I^* for MJ33. These results show that the apparent affinity for the substrate DC_7PC increases up

Table 2: Apparent Kinetic Parameters[a] for the Hydrolysis of DC_7PC Micelles[a]

PLA2 (bovine) # mutant	K_I^* MJ33	in 1 mM NaCl				in 4 M NaCl			
		K_M^{app}	V_M^{app}	$X_I(50)$	K_M^*	K_M^{app}	V_M^{app}	$X_I(50)$	K_M^*
1. WT	0.009	2.3	32	0.013	2.2	0.16	700	0.02	0.8
2. K53M	0.004	1.6	200	0.013	0.44	0.13	1000	0.016	0.33
3. K56M	0.0007	0.6	350	0.015	0.047	0.14	1000	0.024	0.03
4. K53,56M	0.0006	0.55	310	0.025	0.026	0.07	600	0.06	0.011
5. K120,121A	0.0015	1	31	0.007	0.27	0.13	350	0.014	0.12
6. K53,56,120M	0.0003	0.69	460	0.03	0.01	0.12	940	0.05	0.006
7. K53,56,121M	0.0007	0.5	420	0.023	0.031	0.11	750	0.059	0.012
8. K53,120,121M	0.0004	1.7	90	0.01	0.042	0.08	420	0.022	0.019
9. K56,120,121M	0.0003	0.8	210	0.011	0.028	0.07	660	0.04	0.008
10. K53,56,120,121M	0.0004	0.36	460	0.032	0.013	0.12	750	0.065	0.006
venom nmDEI	nd	0.42	120	0.017		0.31	132	0.021	
nmDEII	nd	0.31	300	0.03		0.28	435	0.05	
nm DEIII	nd	0.65	2400	0.03		0.20	1940	0.065	
appPLA2	nd	0.1	1170	0.02		0.26	2600	0.025	

[a] Uncertainty in these values is 30%. Results in the first five rows are from Rogers et al., 1998; Yu et al., 1999).

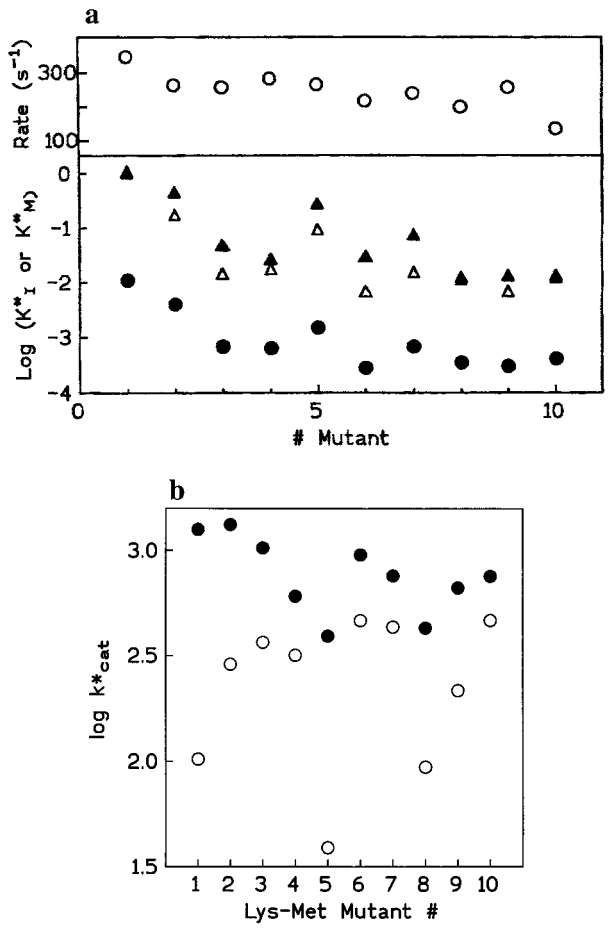

FIGURE 2: (a) (Bottom panel) The binding parameters (on a log scale) for the lysine substitution mutants of bovine PLA2: (filled circle) K^*_M for MJ33, (open triangle) K^*_M for DMPM vesicles, (filled triangles) DC_7PC micelles in 1 mM NaCl. (Top panel) Initial rate of hydrolysis of DMPM vesicles by the lysine substitution mutants. (b) The k^*_{cat} values for the hydrolysis of DC_7PC micelles by lysine substitution mutants (# from Table 2) in the presence of 1 mM (open circles) or 4 M NaCl (filled circles) at pH 8.0 in the presence of 10 mM $CaCl_2$.

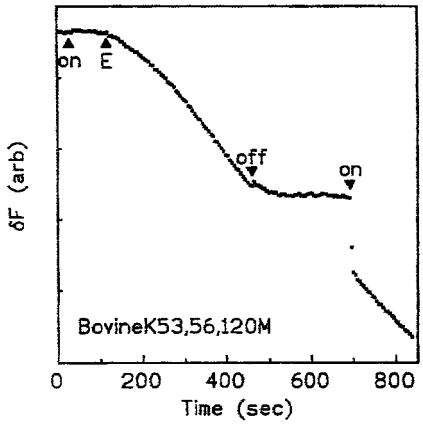

FIGURE 3: Reaction progress for the hydrolysis of DC_6PC (0.44 mM) by K53,56,120M mutant of bovine PLA2 monitored as the change in the fluorescence emission (*41*). This protocol is useful for eliminating the contribution of the reaction on cuvette walls. The reaction progress is monitored as a change in the fluorescence emission intensity of a pH-indicator dye. The protons released at the extraneous interfaces are brought into the beam path only if the solution is stirred. Otherwise, self-diffusion from the walls to the edge of the observation window in the center of the cuvette takes several minutes. The reaction progress with stirring off is barely above the background. The accumulated product is brought into the beam paths as soon as the stirring is turned on again. These results show that virtually all the observed reaction occurs at the walls.

to 100-fold by the lysine substitutions. Together, as summarized in Figure 2panel A, the lysine substitutions cause a significant increase in the affinity for the active site directed DMPM, DC_7PC, and MJ33, as well as for deoxy-LPC (see below). V^{app}_M for most mutants are in a 3-fold range for DTPM (Figure 2, panel A) or for DC_7PC in 4 M NaCl (Table 2). However, as plotted in Figure 2, panel B, the effect of added NaCl on k^*_{cat} for DC_7PC decreases by lysine substitution; however, such effects clearly depend on the position of the residue. These results will be used to obtain the magnitude of the incremental changes affected by specific substitutions.

Other observations related to the issue of the charge compensation at the interface are also summarized in Table 2. The apparent parameters for the hydrolysis of DC_7PC micelles by the venom PLA2 show that a modest salt effect on V^{app}_M is seen only with appPLA2 which has Lys-56 (Table 1). In contrast, the three isozymes of nmPLA2, which do not have cationic residues in positions 53, 56, 120, 121 do not show the salt effect. Note that the isoelectric points of these enzymes are in the 5 to 9 range (*45*), and they have 10−15 cationic residues (*27*, *35*). These results suggest that specific cationic residues, rather than the net charge on PLA2, control the anionic charge preference.

Only the Turnover at the Zwitterionic Interfaces is Influenced by the Lysine Substitutions. As shown in Figure 1, the observed rate below the CMC of DC_7PC changes modestly for the K53,56,120M triple mutant. Such sub-cmc rates, measured under the vigorously stirred pH-stat conditions, have been interpreted as the classical catalytic turnover through the decomposition of monomer ES complex in the aqueous phase (*17*, *27*, *40*). These rates have a significant contribution from the PLA2-catalyzed reaction on the surface of air bubbles and the vessel walls (*41*). As shown in Figure 3, the fluorescence change virtually ceases as soon as the stirring is turned off. As stirring is turned on again, after a burst of the fluorescence change the reaction continues with the same rate as before the stirring was turned off. On the basis of the slope of the fluorescence change with stirring off, the turnover rate for the K53,56,120M mutant is <0.1 s^{-1}, as it is for WT (*41*). These results clearly rule out an effect of lysine substitutions on the catalytic turnover through monodisperse ES in the aqueous phase.

Effect of the Lysine Substitution on the Hydrolysis of Phosphatidylcholine Vesicles. The initial rate of hydrolysis of zwitterionic vesicles by pancreatic PLA2 is very slow. As summarized in Table 3 (columns 3 and 4), the rate of hydrolysis of DOPC vesicles by WT increases 10-fold in the presence of 4 M NaCl. For the substitution mutants, the rates in 1 mM NaCl increase up to 10-fold, yet the rates in the presence of 4 M NaCl are between 30 and 40 s^{-1}. These results show that added NaCl or the lysine substitutions increase the rate of DOPC hydrolysis; however, a low processivity for the interfacial turnover precludes detailed analysis (*1*, *2*, *6*).

Reaction progress for the hydrolysis of DMPC vesicles by WT exhibits a delay to the onset of a sustained reaction

Table 3: Observed Rates (s^{-1}) of Hydrolysis of DOPC or DMPC Vesicles[a]

PLA2 (bovine) # mutant	with DOPC		with DMPC in 1 mM NaCl	
	1 mM NaCl	4 M NaCl	delay (min)	rate
1. WT	4	42	13.5	41
2. K53M	6	34	10.7	32
3. K56M	9.5	36	6.1	54
4. K53,56M	31	34	5	75
5. K120,121A	5.3	29.4	12.1	39.3
6. K53,56,120M	27.3	40	5.3	86
7. K53,56,121M	36	36	5.5	93
8. K53,120,121M	6.3	27.3	10.8	43
9. K56,120,121M	33.6	33.6	9.1	61
10. K53,56,120,121M	26	27	6.3 (<1)	72 (140)
12. nmPLA2 DEI	27	56	<0.5	23
13. nmPLA2 DEII	80	17	<0.5	38
14. nmPLA2 DEIII	168	47	<0.5	185

[a] Uncertainty in these values is 10%. The delay and steady rate are measured with 0.3 mM DMPC or DOPC at 23 °C in 1 mM NaCl, Ca^{2+} 10 mM. Values in parentheses are in 4 M NaCl.

progress. The delay for WT is completely lost in DMPC vesicles containing about 8% products or in the presence of 4 M NaCl (results not shown) (*4*, *39*). The delay time and the sustained maximum rate for the substitution mutants are summarized in Table 3 (columns 5 and 6). As expected, only a modest effect of the lysine substitution is seen on the rate because the bound form of the enzyme is charge-compensated. However, a residual charge effect is much more obvious in the observed delay time of 5 min for the triple mutant as compared to no detectable delay time for the nmPLA2 DE1 (Table 3). Together, lysine-53, -56, and -120 in WT bovine pancreatic PLA2 account for about a 30-fold k^*_{cat} enhancement at the anionic interface. A modest residual salt activation and the delay suggest that the triple mutant is not as fully charge-compensated at the zwitterionic interface as it is at the anionic interface.

Crystal Structure of K53,56M Mutant. The refinement and stereochemical parameters for the final crystallographic structure of K53,56M double mutant are given in Table 4. The average isotropic temperature factors of the main chain atoms, the side chain atoms, the calcium ion, and the 106 water molecules are given. The coordinate error is estimated to be 0.2 Å (*46*). The stereochemical quality of the final protein model was checked by the program PROCHECK (*47*). Ninety-one percent of the residues are in the most favored regions of the Ramachandran plot (*48*), and the remaining residues are in the additional allowed region.

As shown in Figure 4, the overall backbone folding and other features of the tertiary structure are virtually identical in the WT and the double mutant. Both structures are obtained from the isomorphous trigonal forms, which means that if any difference is found it cannot be attributed to the crystal packing constraints. The backbone atoms (492 atoms) superimpose with a root-mean-square (rms) deviation of 0.26 Å, and it is 0.18 Å if the disordered surface loop residues 62−68 are omitted. The active site cleft consists of the five water molecules including the conserved structural water hydrogen bonded to the N-terminus. All the atoms of the active site residues Ala-1, His-48, Asp-49, Tyr-52, Asp-99, the conserved structural and catalytic waters attached to Nδ1 of His-48 superimpose well with the deviation of 0.14 Å. In both cases, the calcium ion has seven ligands in a pentagonal

Table 4: Crystallographic and Relevant Geometrical Parameters for Bovine K53,56M PLA2

unit cell parameters	$a = b = 46.41$ Å and $c = 102.72$ Å
space group	$P3_121$
resolution range	10.0−1.9 Å
total no. of observations	42 068
unique reflections	9733
R_{merge} (%)[a]	9.2
cumulative completeness at 1.9 Å	89%
R_{work}(%) for 8033 reflections	18.9
R_{free} (%) for 949 reflections	22.4
parameter file (X-PLOR)	parhcsdx.pro
topology file (X-PLOR)	tophcsdx.pro
protein model (PDB-ID 1C74 atomic coordinates) and R1C74SF	
protein atoms	955
bound calcium ion	1
water molecules	106
RMS deviation from ideal bond lengths	0.011 Å
RMS deviation from ideal bond angles (deg)	1.561
RMS deviation from ideal dihedral (deg)	22.7
RMS deviation from ideal improper (deg)	1.17
average atomic temperature factors of the refined model (Å^2)	
main-chain atoms	20.8
side-chain atoms	25.1
water molecules	32.8
calcium ion (Ca^{2+})	16.9

[a] $R_{merge} = \Sigma_{hkl}| I - \langle I\rangle |/\Sigma I$, where I is the observed intensity and $\langle I\rangle$ is the average intensity from observations of symmetry-related reflections, respectively.

bipyramidal coordination with the ligand distances in the 2.21 to 2.65 Å range with an average distance of 2.40 Å. The backbone structure does not change in the presence of MJ33 in WT (*49*), and docking of MJ33 with energy minimization into the K53,56M mutant did not cause any noticeable change.

Disordered residue Pro-68 is not included in the superposition calculation. The electron density in general is clearer for most regions for the protein model except for the [62−68] loop. As shown in Figure 4, panel A, in addition to the modest difference in the [62−68] loop, the following changes in the side chains are of particular interest: (a) All the atoms of the calcium [27−33] loop residues superpose very well except the side chain atoms of Leu-31. (b) The side chain atoms of 10 residues (Leu-2, Trp-3, Lys-10, Leu-19, Asn-24, Leu-31, Tyr-69, Asn-79, Glu-87, and Asp-119) of the double mutant are in noticeably different positions as compared to the WT structure. The electron density is not clear for the residues 2, 3, 31, and 69. Note that most of the residues along the bottom plane perpendicular to the paper in Figure 4 are on the surface that putatively makes contact with the substrate interface, i.e., the i-face (*50*). (c) In the N-terminal [1−10] helix the side chains of Leu-2, Trp-3, and Lys-10 are different as compared to WT. This helix lines the substrate binding pocket, and Leu-2 and Trp-3 make contact with the interface.

Earlier we had published the structure of the K120,121A mutant (1C74) of bovine PLA2 (*20*). As shown in Figure 4, panel B, its backbone structure is essentially identical to that of WT (1MKT). However, side chains of several residues of the i-face (residues 2, 3, 10, 19, 24, 119) are different. In addition, there is a significant difference in the conformation of the side chains of residues 43, 53, 56, 57, 81, 100, 108, 113. Together, the changes emphasized in Figure 4, panels A and B, suggest that the changes resulting from the lysine

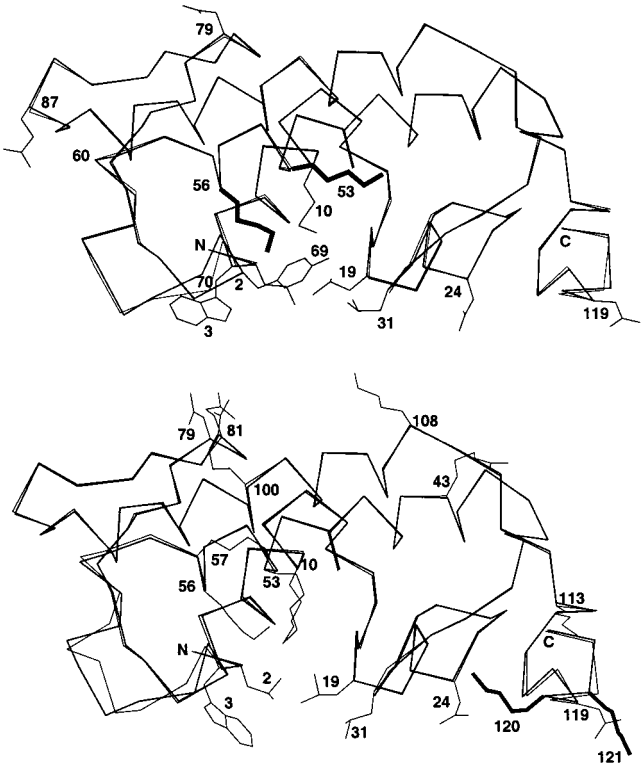

FIGURE 4: (A) Backbone superposition of K53,56M (1C74, heavy line) on isomorphous WT (1MKT). The side chains of K53 and K56 are marked by heavy lines. Only the side chains of the double mutant that differ significantly relative to WT are shown and numbered. (B) The backbone superposition of K120, 121A (1IRB, heavy line) structure (*20*) on isomorphous WT (1MKT). The side chains of K120 and K121 are marked by heavy lines. Only the side chains of the double mutant that differ significantly relative to WT are shown and numbered. This orientation of the enzyme has been suggested to be that at the interface such that the interface plane passes perpendicular to the paper at the lower edge of the structure (*50*). Note that in both cases, most of the residues that show altered side chains are at the i-face that contacts with the interface.

substitution in the double mutant are on the contiguous surfaces of PLA2 that are reasonably well separated from the site of the substitutions. The structural reciprocity between the substitution at 120/121 versus 53/56 is remarkable. The fact that the reciprocity is not observed for all the same residues is also significant. For example, Leu-31 and Tyr-69 control k^*_{cat}, both of which do not change with the 120,121 mutation, which is consistent with the fact that the substitution of these residues has little effect on k^*_{cat}.

Spectroscopic Properties of the Lys-Substitution Mutants. The long-range effects of lysine substitution are also apparent in the environment of the only tryptophan residue in the PLA2. A difference in the microenvironment of Trp-3, as indicated by the crystal structures of WT versus the K53,-56M mutant, is consistent with the absorbance difference in the 290-nm region (Figure 5). Such differences between the WT and the mutants in the aqueous phase show that substitution of 53 or 56 induces identical change; however, it is qualitatively different than that observed with the K120,-121A. Similar changes were also seen in the E form of other substitution mutants. Since these mutation sites are >10Å away from Trp-3, the spectroscopic and X-ray results suggest a long-range structural effect of the lysine-to-methionine substitution.

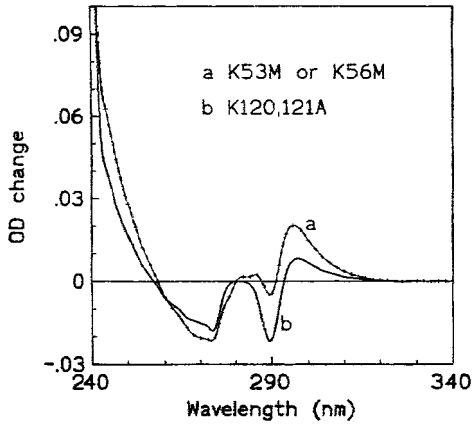

FIGURE 5: UV difference spectra for (a) K53M or K56M (superimposed curves) or (b) K120,121A double mutant relative to WT. These difference spectra were obtained by subtracting the WT spectrum from that of the mutant (both normalized at 280 nm). These measurements were made in 10 mM Tris at pH 8.0

Table 5: Fluorescence Emission Intensities (and K_d in μM for the E* to E Form) of the Various Forms of PLA2 Mutants

mutant	E	ECa	E* (K_d)	E*Ca (K_d)
WT	1[a]	1.22	2.48 (3100)	2.46 (1900)
WT/D_2O	1.67	1.47	3.53 (3050)	
K53,56,120M	1.57	1.62	2.58 (136)	2.58 (66)
K53,56,120M/D_2O	1.68	1.56		3.57 (55)
K53,56M	1.43	1.63	2.89 (216)	2.38 (43)
K120,121A	1.32	1.49	2.8 (300)	2.56 (81)

[a] All emission intensities are normalized for the intensity at 350 nm for the WT in aqueous phase. The intensities for the E and ECa forms are at 350 nm and for the E* and E*Ca forms are at 330 nm. All other settings were identical in all cases: excitation at 280 nm with 4-nm slit widths. Standard deviation for the K_d values is 30%.

Table 6: Acrylamide Concentration[a] (mM) for 50% Quenching for the Various Forms of the PLA2 Mutants

mutant	ECa	E*	E*Ca
WT	44		74
K53,56,120M	39	84	96
K53,56M			87
K120,121A			84

[a] Uncertainty in these measurements is 10%. The E* and E*Ca forms are for the enzyme bound to 3 mM deoxy-LPC.

The changes in the fluorescence emission characteristics of K53,56,120M and other mutants were examined under a variety of conditions. Key results are summarized in Tables 5 and 6. The normalized intensities in Table 5, relative to the E form of WT in the aqueous phase, show that the maximum emission intensities are sensitive to the environment as well as to the events at the active site and the i-face. For example, the peak emission intensity increases on the calcium binding, and as shown in Figure 6 the calcium-induced change in the emission spectrum for the WT is different than it is for the triple mutant. Such differences induced by the calcium binding to the enzyme in the aqueous phase suggest that the Trp-3 environment is influenced by the lysine substitutions.

The changes in the Trp-3 fluorescence emission spectrum induced in the presence of deoxy-LPC micelles are compared in Figure 7. Except for a difference in the magnitude of the change at a given deoxy-LPC concentration, virtually identi-

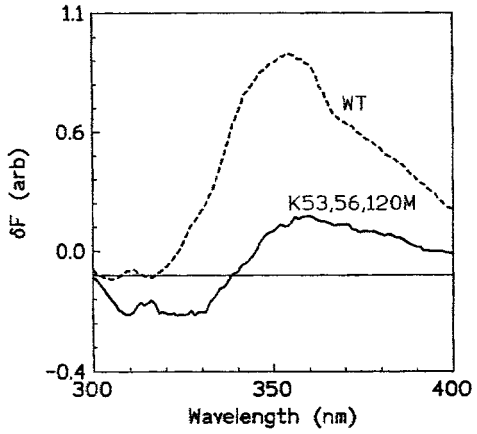

FIGURE 6: The (10 mM) calcium-induced change in the fluorescence spectra for the WT or the triple mutant in the aqueous phase with 10 mM Tris at pH 8.0.

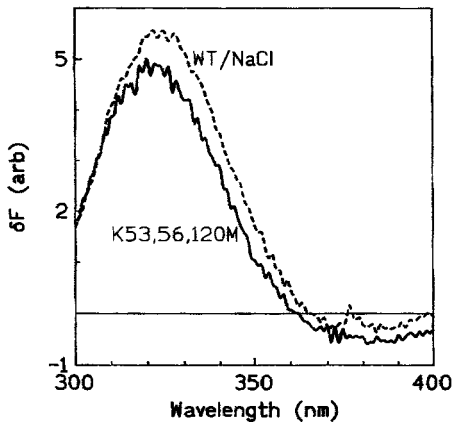

FIGURE 7: Deoxy-LPC induced fluorescence emission spectra for the triple mutant or WT with 4 M NaCl. These measurements were made in 10 mM Tris at pH 8.0.

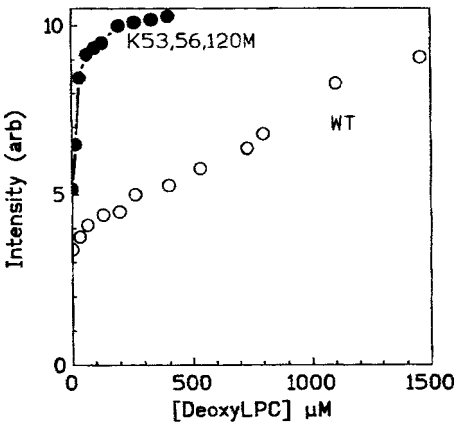

FIGURE 8: Fluorescence emission intensity of WT or the triple mutant at 333 nm as a function of deoxy-LPC concentration. Other conditions as in Figure 7.

cal spectral change is induced in the triple mutant or the WT in the presence of NaCl. As shown in Figure 8, the increase in the intensity depends on the concentration of deoxy-LPC. These results clearly show that the affinity of the triple mutant for the zwitterionic interface is considerably higher relative to that for WT. The K_d values for the E* forms (Table 5) under several conditions were obtained with fit to a single hyperbola. However, as apparent from the results in Figure 8, the fit for the WT is poor ($r = 0.9$), and there are also other indications that the underlying binding process involves two steps (not shown). The K_d values summarized in Table 5 show that the affinity of the mutants for the zwitterionic interface is considerably higher, as also suggested by its relation (eq 2) to the kinetically obtained K_M^{app} values (Table 2). These results show that substitution of Lys-53,56,120 by Met increases the affinity of PLA2 for the zwitterionic interface by a factor of 25. Note that an apparently lower K_d value for the E*Ca form is most likely due to the calcium-dependent affinity of deoxy-LPC for the active site of the triple mutant.

The maximum intensities for the bound forms of all the mutants approach a value of 2.6 (Table 5). These results suggest that although the Trp-3 environment in the aqueous phase differs noticeably for the various mutants, the environment is comparable for all mutants bound to the interface in the charge-compensated E* or E*Ca forms. Also note that the maximum intensity in the D_2O medium is about 3.5. This difference in the intensities in H_2O versus D_2O is attributed to a difference in the accessibility of E* to water through solvation or the bulk environment (*51*). Accessibility of Trp-3 from the bulk aqueous phase was monitored by acrylamide quenching. As summarized in Table 6, the acrylamide concentration for 50% quenching increases by a factor of 2.5 for the E* and E*Ca forms. Together, the quenching results suggest that while the E*Ca form on the zwitterionic interface is shielded from the dynamic collisional quenching by acrylamide, Trp-3 in the E* form at the zwitterionic deoxy-LPC interface is still accessible to water, possibly through a hydrogen-bonding interaction with the NH of indole.

DISCUSSION

It is remarkable that only 3 out of the 12 cationic residues of bovine IB PLA2 account for virtually all the interface binding, which together with k_{cat}^* activation by the interfacial anionic charge forms the basis for the anionic interface preference. We attribute the lower rates at the zwitterionic interface to a lower affinity for the interface and to a lower partitioning of the Michaelis complex into a catalytically inert E*S form. Although the basis for the residual delay at the zwitterionic bilayer interface (Table 3) is still unresolved, all other results leave little doubt that the anionic interface preference of the pancreatic enzyme is virtually completely mediated by Lys-53,56,120. The loss of the anionic interface preference in K53,56,120M mutant of bovine PLA2 imparts kinetic characteristics that are remarkably similar to those for the snake enzyme (*38*). Together these results provide a structural basis for understanding the interface preference of the PLA2 isoforms.

Specific considerations of the observed k_{cat}^* allosteric effects of the interfacial anionic charge are developed below in terms of the two-state model outlined in the introduction. The binding of PLA2 to the interface is a prelude for the processive interfacial catalytic turnover. In this step, the i-face of E* makes a contact with the organized substrate interface. As a first-order approximation, the bound enzyme has been assumed to be a single species that undergoes the substrate binding and chemical step for the catalytic cycle. A need for an additional step to control the turnover at the interface was anticipated (*4*). Now to account for the allosteric k_{cat}^* activation, we propose that the charge on the interface controls the equilibrium between the two forms of the ternary

Michaelis complex. Note that this extra step does not change our kinetic interpretations (*1*, *3*, *6*) but only allows a further dissection of the parameters as shown in eqs 4 and 5.

The E to E step*. Virtually all methods for the characterization of the enzyme species at the interface have varying contributions from the sequential steps associated with the binding of substrate and/or its mimics to the bound enzyme. Such contributions are eliminated at the deoxy-LPC interface, a zwitterionic neutral diluent with little affinity for the active site of E* (*7*). The K_d values for the calcium free form of E* clearly show a 25-fold increase in the affinity of the triple mutant (Table 5), which is consistent with the electrostatic compensation of three charges. We believe that additional factors are also at work in the stability of E* at the anionic interface. Recall that the affinity of PLA2 for the anionic substrate interface in the absence of calcium is larger by several orders of magnitudes, with an upper limit estimate of $K_d < 1\ \mu$M (*2*, *4*). Attempts to resolve such factors are in progress.

The Chemical Step Remains Unchanged. It appears that the anionic charge has multiple effects. The analysis developed below shows that the charge compensation of certain cationic residues by the interfacial anionic charge is the basis for the k^*_{cat} allosteric effect, and a conformational component is also discernible in the substitution mutants. In the two-state model, the chemical step occurs only through the $(E^*S)^\#$ form which predominates at the anionic interface. Therefore, factors that change $K^\#$ will not necessarily change the reaction mechanism. This assertion is supported by the observation that the ratio of the rates of hydrolysis of the *sn*-2-oxy versus the *sn*-2-thio analogues of DMPM or DC_7-PC in 1 mM or 4 M NaCl remains about 10 for all the mutants (results not shown), as is the case with WT (*52*). The oxy versus thio element effect of this magnitude is attributed to the decomposition of the tetrahedral intermediate in the chemical step as the rate-limiting step (*53*, *54*). The fact that the element effect is not altered, even though the absolute rates change with added NaCl or with the lysine substitutions, is consistent with the assumption that the underlying catalytic mechanism in the chemical step remains unchanged.

Origin of the k^*_{cat} Activation. The observation that K^*_M and K^*_I are virtually independent of salt concentration (as also shown in ref *6*) shows that the charge compensation has little or no direct effect on the mimic binding properties of the bound enzyme. The parameters for the two-state model are defined by eqs 4 and 5. In the two-state scheme, the substrate binding is independent of the conformation, or the species $E^\#$ or $(E^*S)^\#$ are not present in any significant amounts for the WT at the zwitterionic interface. This suggests that the charge neutralization by itself does not influence the enzyme conformation, at least in the E* and E*S forms. Thus, the interfacial anionic charge acts either by stabilizing the active $(E^*S)^\#$ complex by lowering $K^\#$ or directly by stimulating the catalytic rate (k_2).

$$k_{cat} = \frac{k_2}{1 + K^\#} \tag{4}$$

$$K^*_M = \frac{K^\# K^*_S}{1 + K^\#} \tag{5}$$

Table 7: Effects of Mutation on Rate Activation and Stability of Michaelis Complex (Eqs 4−6)[a]

# mutant	K_{charge}	$\Delta_m G^*_S$	$\Delta_m(G^\# - G^*_S)$
1. WT	1	0	0
2. K53M	2.7	−0.5	0.0
3. K56M	4.4	−1.9	0.1
4. K53,56M	6.5	−2.5	0.4
5. K120,121A	1.2	−1.1	0.7
6. K53,56,120M	6.0	−2.9	0.2
7. K53,56,121M	7.0	−2.5	0.3
8. K53,120,121M	2.7	−2.2	0.6
9. K56,120,121M	4.0	−2.7	0.4
10. K53,56,120,121M	7.6	−2.9	0.3

[a] Column 2: Effect of charge neutralization for each mutant on the catalytic rate at low salt (-fold increase over WT); from eq 8. Column 3: Effect of mutation on the binding free energy (stability) of the E*S complex (kcal/mol) from eq 6 evaluated at high salt. Similar numbers are found at low salt. Column 4: Effect of mutation on the stability of the $(E^*S)^\#$ complex above the change on E*S (kcal/mol) from eqs 6 and 7 evaluated at high salt where the charge-compensation effects do not contribute.

On the basis of the above consideration, we can subdivide the effects of the mutations into a charge compensation effect and a charge-independent conformational effect. The salt dependence of k^*_{cat}, and a lack of the salt effect on K^*_M, suggests that $K^*_M = K^*_S$ as also argued previously for DC_7PC (*6*). Thus K^*_M can be used to calculate the stability of the E*S complex. Thus, on the basis of $K^*_M = K^*_S$ and eq 5, $K^\# \gg 1$, which would imply that $k^*_{cat} = k_2/K^\#$. On the basis of these limits, we analyze the data in Table 2 with the following assumptions applied to the two-state scheme above: (a) If the standard free energy of E* is chosen as zero, the standard free energy of E*S is $G^*_S = -RT \ln(1/K^*_M)$ and that of $(E^*S)^\#$ is $G^\# = -RT \ln(K^\#/K^*_S)$. (b) Charge neutralization, either through mutation or salt addition, influences only the k^*_{cat}. The same maximum charge compensation can be achieved for all mutants by addition of salt or at the anionic interface. (c) In addition to the charge compensation, mutations also influence the stability of both E*S and $(E^*S)^\#$ complexes through charge-independent effects on enzyme conformation.

The standard free energy changes from mutations (m) at high (H) or low (L) salt can be calculated as

$$\Delta_m G^*_S = \ln\left(\frac{K^*_M(\mathrm{m})}{K^*_M(\mathrm{WT})}\right) \tag{6}$$

for the stability of the E*S complex and

$$\Delta_m G^\# = -\ln\left(\frac{k^*_{cat}(\mathrm{m})}{k^*_{cat}(\mathrm{WT})}\frac{K^*_M(\mathrm{WT})}{K^*_M(\mathrm{m})}\right) \tag{7}$$

for the stability of the $(E^*S)^\#$ complex.

At high salt, charge neutralization is already maximal (by assumption b above) and all changes in the free energy levels refer only to the binding properties of the two states. At high salt, the mutations leave k^*_{cat} fairly invariant suggesting that they affect the stabilization of E*S and $(E^*S)^\#$ in roughly the same way. However, there are some systematic deviations such that $\Delta_m G^\#$ is larger (between 0 and 0.7 kcal/mol, Table 7) than $\Delta_m G^*_S$ in almost all cases. This suggests that the

mutations do not stabilize $(E^*S)^{\#}$ quite as much as E*S, as if the mutations bring the E* form somewhat closer to the substrate-binding conformation than to the active conformation $E^{\#}$. It is as though some transition-state stabilization effect in the WT is relaxed in the mutants; however, this effect is small. Also note that virtually all substitutions always further stabilize the E*S state, although the effect on the free energy is not additive.

By assumption c above, the changes in the active site binding properties when mutations are added are the same at high and low salt. Consequently, by dividing out the binding effects calculated from the high salt data from the results at low salt, we can estimate the charge neutralization effect at low salt for each mutant m:

$$K_{\text{charge}} = \frac{k^*_{\text{cat}}\,(\text{m, L})}{k^*_{\text{cat}}\,(\text{WT, L})}\,\frac{k^*_{\text{cat}}\,(\text{WT, H})}{k^*_{\text{cat}}\,(\text{m, H})} \qquad (8)$$

This gives a very clear separation of the mutants into classes determined by the presence or absence of mutations at positions 53 and 56 (Table 7). Those with no mutation at either 53 or 56 (i.e., #5) have $K_{\text{charge}} = 1.2$, those with only 53 (i.e., #2 and #8) have $K_{\text{charge}} = 2.7$, those with only 56 (i.e., #3 and #9) have $K_{\text{charge}} = 4.0-4.4$, and those with both 53 and 56 (i.e., #4, #6, #7, and #10) have $K_{\text{charge}} = 6.0-7.6$. These numbers correspond to the factor with which k^*_{cat} increases due to the charge neutralization alone after the effect on binding has been factored out. This increase could be due either to a stabilization of the active complex or to a direct stimulation of the catalytic rate. The presence or absence of mutations at positions 120 and 121 show no systematic effect on K_{charge}.

The clear separation of the substitution effects on K_{charge} supports the assumptions on which the calculation was based. Although the model cannot be proven in this way, it is consistent with the kinetic data. The analysis suggests that Lys-53 and Lys-56 have strong charge-compensation effects, while 120 and 121 do not. However, 120/121 do contribute to conformational changes in the protein that strengthens substrate binding and decreases k^*_{cat}. The main effect of removing the charged residues at 120/121 may be to strengthen the interface binding and lower K^*_S of the enzyme at the zwitterionic interface. In short, our analysis shows that the substitution of specific residues contributes differentially toward K_d, $K^{\#}$, K^*_M, and k_2.

The Structural Basis for the Anionic Interface Preference and Other Events at the i-Face. It is now becoming increasingly clear that the i-face has evolved to make close molecular contact with the substrate interface. Such a contact brings the molecules within 2.4−4 Å for the desolvation of the microinterface (*50*, *51*). The thermodynamic and functional coupling of the structural changes associated with the interfacial binding and the catalytic events requires a better understanding of the i-face. The idea of the thermodynamic and structural reciprocity is consistent with the allosteric changes induced through the i-face. It is also relevant that a Trp-31 substituent on PLA2, although not a residue on the i-face, clearly discerns a difference in zwitterionic versus anionic interfaces (*66*). Such propensities of the overall structure to adopt to the potential structural irregularities at the interface implies that ensemble of closely related structures in equilibrium may coexist in the solution as well as at the interface. If so, the challenge is to ascertain which factors stabilize a particular structure and how it relates to a functionally relevant state of the enzyme.

How the effects of the charge and conformation are mediated also remains to be sorted out. Although consistent with the two-state model, the k^*_{cat} allosteric effect remains to be rationalized in terms of the catalytic mechanism for the chemical step. If we describe $(E^*S)^{\#}$ as the transition-state complex, we must also accept that the tetrahedral mimic is not very close to this transition-state conformation since K^*_I is salt-independent and the value is dominated by E*I. This conclusion is entirely consistent with the calcium-coordinated oxyanion mechanism (*53*, *54*) in which the rate-limiting transition state is during the decomposition of the tetrahedral intermediate.

Charge Compensation versus Surface Electrostatics. Interfacial anionic charge plays a significant role in the binding of numerous proteins to interfaces (*60*, *61*), yet adequate structural and functional models to evaluate such interactions remain to be established. As evaluated below significant insights can be gained from the results of the two orthogonal site-directed mutagenesis approaches for understanding the anionic charge preference of PLA2.

On the basis of the surface electrostatics model for the interaction between the i-face and the anionic interface (*62*), Gelb and co-workers designed the charge-reversal mutants with the cationic residues replaced by anionic glutamate (*63*−*65*). Up to a 20-fold increase in K_d was observed, which is consistent with the K_d for the triple mutant of the pancreatic PLA2 at the zwitterionic interface decreases by a factor of 25 (Table 5). However, the charge-reversal mutants do not show a dramatic decrease in the activity at the anionic interface, as if the expected long-range electrostatic charge repulsion does not occur. Not only can the mutants away from the interface not provide information about the enzyme at the interface, a negative outcome from the charge-reversal mutants only suggests that other interactions may dominate the contact between the i-face and the interface including a shift in the pK_a of the glutamates.

In contrast, the mutants for the present study were designed on the basis of our model for the close contact of the i-face where the anionic interface selectively charge-compensates certain cationic residues as a prelude for the optimal hydrogen-bonding and hydrophobic interactions (*50*, *51*). This model implies a specificity of the interactions along the i-face through close contacts. Thus, the isosteric lysine-to-methionine substitution not only charge compensates but also retains the propensity for the subsequent close contacts (*9*). In short, the anionic interface preference is the end result of a complex set of atomic level interactions of the PLA2 isoforms, which we are trying to sort out in collaboration with Professors Bahnson and Gelb.

Evolutionary and Physiological Significance. A preference of the pancreatic PLA2 for an anionic interface reflects an evolutionary adaptation for the physiological environment of the digestive tract in higher animals where the phospholipid substrate is codispersed with dietary lipids and bile salts (*55*). A comparison of the properties of K53,56,120M mutant of bovine IB PLA2 with the *Naja* venom IA PLA2 implies that successful evolution of the anionic interface preference

has occurred through the mutation of only a few well-positioned residues. Thus our analysis is also of interest for evaluating the interface preferences of the evolutionarily divergent secreted PLA2 isoforms with His−Asp and calcium at the catalytic site (*27*, *35*, *43*). For example, seven PLA2 isoforms are expressed in humans (*56*−*58*); however, their detailed tertiary structure, active site geometry, kinetic properties, and cellular functions remain to be established. It is not unlikely that a key functional difference is in their anionic interface preference, as also suggested by the fact that the patterns of the cationic residues at 53, 56, and 120 positions are somewhat different in the isoforms. The significance of a modest difference in the anionic charge preferences of the PLA2s present in the physiological milieu can be large enough to selectively target membrane of certain cell types but not the others. For example, anionic charge on the outer surface of the plasma membrane could develop in response to a signal, such as the transbilayer translocation of an anionic phospholipid or the accumulated product in response to the activation of cytoplasmic PLA2. In addition, secreted PLA2 also interacts with heparin and glycoconjugates of endothelial surfaces, possibly through the cationic residues away from the i-face (*59*). Together such a diversity of interactions of PLA2 make them amenable to control and regulation through a variety of mechanisms for the distribution in the various compartments of a cell.

ACKNOWLEDGMENT

We gratefully acknowledge numerous critical discussions spanning more than a decade with Professor Michael H. Gelb (Seattle) on the various incarnations of the problem of interfacial activation. The facilities of the Bioinformatics Centre, Interactive Graphics based Molecular Modeling, Super Computer Education and Research and the National Area Detector at Molecular Biophysics Unit (all at IISc, Bangalore, India) are gratefully acknowledged.

REFERENCES

1. Berg, O. G., Yu, B.-Z., Rogers, J., and Jain, M. K. (1991). *Biochemistry 30*, 7283−7297.
2. Jain, M. K., Gelb, M. H., Rogers, J., and Berg, O. G. (1995). *Methods Enzymol. 249*, 567−614.
3. Gelb, M. H., Jain, M. K., Hanel, A. M., and Berg, O. G. (1995) *Annu. Rev. Biochem. 64*, 653−688.
4. Jain, M. K., and Berg, O. G. (1989) *Biochim. Biophys. Acta* 1002, 127−156.
5. Jain, M. K., Yu, B.-Z., and Berg, O. G. (1993) *Biochemistry*, *32*, 11319−11329.
6. Berg, O. G., Rogers, J., Yu, B., Yao, J., Romsted, L. S., Jain, M. K. (1997) *Biochemistry*, *36*, 14512−14530.
7. Jain, M. K., Yu, B.-Z., Rogers, J., Ranadive, G. N., and Berg, O. G. (1991) *Biochemistry 30*, 7306−7317.
8. Yu, B. Z., Ghomashchi, F., Cajal, Y., Annand, R. R., Berg, O. G., Gelb, M. H., and Jain, M. K. (1997) *Biochemistry 36*, 3870−3881.
9. Rogers, J., Yu, B. Z., Tsai, M. D., Berg, O. G., and Jain, M. K. (1998) *Biochemistry 37*, 9549−9556.
10. Jain, M. K., Rogers, J., Berg, O., and Gelb, M. H. (1991) *Biochemistry 30*, 7340−7348.
11. Cajal, Y., Rogers, J., Berg, O. G., and Jain, M. K. (1996) *Biochemistry 35*, 299−308.
12. Cajal, Y., Ghanta, J., Surolia, A. K., Easwaran, E., and Jain, M. K. (1996) *Biochemistry 35*, 5684−5695.
13. Cajal, Y., and Jain, M. K. (1997) *Biochemistry 36*, 3882−3893.
14. Noel, J. P., Bingman, C. A., Deng, T., Dupureur, C. M., Hamilton, K. J., Jiang, R., Kwak, J., Sekharudu, C., Sundaralingam, M., and Tsai, M. D. (1991) *Biochemistry 30*, 11801−11811.
15. Lugtigheid, R. B., Otten-Kuipers, A. A., Verheij, H. M., and de Haas, G. H. (1993) *Eur. J. Biochem. 213*, 517−522.
16. Lugtigheid, R. B., Nicolaes, C. A. F., Veldhuizen, E. J. A., Slotboom, A. J., Verheij, H. M., and de Haas, G. H. (1993) *Eur. J. Biochem. 216*, 519−525.
17. Verger, R., and DeHaas, G. H. (1976) *Annu. Rev. Biophys. Bioeng. 5*, 77−117.
18. Snitko, Y., Han, S. K., Lee, B. I., and Cho, W. (1999) *Biochemistry 38*, 7803−10.
19. Lee, B. I., Dua, R., and Cho, W. (1999) *Biochemsitry 38*, 7811−7818.
20. Huang, B., Yu, B. Z., Rogers, J., Byeon, I. J., Sekar, K., Chen, X., Sundaralingam, M., Tsai, M. D., and Jain, M. K. (1996) *Biochemistry 36*, 12164−12174.
21. Liu, X.-H., Zhu, H.-X., Huang, B.-H., Rodgers, J., Yu, B.-Z., Kumar, A., and Jain, M.-K., Sundaralingam, M., and Tsai, M.-D. (1995) *Biochemistry 34*, 7322−7344.
22. Li, Y., and Tsai, M.-D. (1993) *J. Am. Chem. Soc. 115*, 8523−8526.
23. Zhu, H.-X., Dupureur, C. M., Zhang, X.-Y., and Tsai, M.-D. (1995) *Biochemistry 34*, 15307−15314.
24. Deng, T., Noel, J. O., and Tsai, M.-D. (1990) *Gene 93*, 229−234.
25. Jain, M. K., Tao, W., Rogers, J., Arenson, C., Eibl, H., and Yu, B.-Z. (1991) *Biochemistry 30*, 10256−10268.
26. Yu, B.-Z., Berg, O. G., and Jain, M. K. (1993) *Biochemistry 32*, 6485−6492.
27. Verheij, H. M., Slotboom, A. J., and de Haas, G. H. (1981) *Rev. Physiol. Biochem. Pharmacol. 91*, 91−203.
28. Sekar, K., Sekharudu, C., Tsai, M.-D., and Sundaralingam, M. (1998) *Acta Cryst. D54*, 342−346.
29. Otwinowski, W. (1993) *Proceedings of the CCP4 Study Weekend*, pp 56−62, Daresbury Laboratory Warrington, UK.
30. Minor, W. (1993) *XDISPLAYF Program*, Purdue University.
31. Brunger, A. T. (1992) *Nature* (London) *355*, 472−474.
32. Brunger, A. T. (1992) *X-PLOR Manual. Version 3.1*. Yale University, New Haven, CT.
33. Jones, T. A. (1985) *Methods Enzymol. 115*, 157−171.
34. Bernstein, F. C., Koetzle, T. F., Williams, G. J. B., Meyer, E. F., Jr, Brice, M. D., Rodgers, J. R., Kennard, O., Shimanouchi, T., and Tasumi, M. (1977) *J. Mol. Biol. 112*, 535−542.
35. Van den Bergh, C. J., Slotboom, A. J., Verheij, H. M., and De Haas, G. H. (1989*) J. Cell. Biochem. 39*, 379−390.
36. Cajal, Y., Berg, O. G., and Jain, M. K. (2000) *Langmuir 16*, 252−257.
37. Bayburt, T., Yu, B. Z., Lin, H., Browning, J., Jain, M. K., and Gelb, M. H. (1993) *Biochemistry 32*, 573−582.
38. Jain, M. K., Egmond, M. R., Verheij, H. M., Apitz-Castro, R. J., Dijkman, R., and de Haas, G. H. (1982) *Biochim. Biophys. Acta 688*, 341−348.
39. Apitz-Castro, R. J., Jain, M. K., and de Haas, G. H. (1982) *Biochim. Biophys. Acta 688*, 349−356.
40. De Haas, G. H., Bonsen, P. P. M., Pieterson, W. A., and Van Deenen, L. L. M. (1971) *Biochim. Biophys. Acta 239*, 252−266.
41. Yu, B. Z., Berg, O. G., and Jain, M. K. (1999) *Biochemistry 38*, 10449−10456.
42. Ortiz, A. R., Pisabarro, M. T., Gallego, J., and Gago, F. (1992) *Biochemistry 31*, 2887−2896.
43. Valentin, E., Ghomaschci, F., Gelb, M. H., Luzdunski, M., and Lambeau, G. (1999) *J. Biol. Chem. 274*, 31195−31202.
44. Yu, B. Z., Rogers, J., Tsai, M. D., Pidgeon, C., and Jain, M. K. (1999) *Biochemistry 38*, 4875−4884.
45. Van Eijk, J. H., Verheij, H. M., Dijkman, R., and de Haas, G. H. (1983) *Eur. J. Biochem. 132*, 183−188.
46. Luzzati, V. (1952) *Acta Cryst. 5*, 802−810.
47. Laskowski, R. A., MacArthur, M. W., Moss, D. S., and Thornton, J. M. (1993) *J. Appl. Cryst. 26*, 283−291.
48. Ramakrishnan, C., and Ramachandran, G. N. (1965). *Biophys. J. 5*, 909−933.

49. Sekar, K., Yu., B.-Z., Rogers, J., Lutton, J., Liu, X., Chen, X., Tsai, M.-D., Jain, M. K., and Sundaralingam, M. (1997) *Biochemistry*, *36*, 3101−3114.
50. Ramirez, F., and Jain, M. K. (1991) *Proteins 9*, 229−239.
51. Jain, M. K., and Vaz, V. L. C. (1987) *Biochim. Biophys. Acta 905*, 1−8.
52. Jain, M. K., Yu, B.-Z. Rogers, J, Gelb, M. H., Tsai, M. D., Hendrickson, E. K., and Hendrickson, S. (1992) *Biochemistry 31*, 7841−7847.
53. Yu, B. Z., Rogers, J., Nicol, G. R., Theopold, K. H., Seshadri, K., Vishveshwara, S., and Jain, M. K. (1998) *Biochemistry 37*, 12576−87.
54. Schurer, G., Lanig, H., and Clark, T. (2000) *J. Phys. Chem. B104*, 1349−1361.
55. Homan, R., and Jain, M. K. (2000) In *Intestinal Lipid Metabolism* (Mansbach, C. M., Tso, P., and A. Kuksis, Eds.) Plenum, NY, in press.
56. Tishfield, J. A. (1997) *J. Biol. Chem. 272*, 17247−17250.
57. Valentin, E., Koduri, R. S., Scimeca, J.-C., Carle, G., Gelb, M. H., Lazdunski, M., and Lambeau, G. (1999) *J. Biol. Chem. 274*, 19152−19160.
58. Suzuki, N., Ishizaki, J., Yokota, Y., Higashino, K., Ono, T., Ikeda, M., Fuji, N., Kawamoto, K., and Hanasaki, K. (2000) *J. Biol. Chem. 275*, 5785−5798.
59. Yu, B. Z., Rogers, J., Ranadive, G., Baker, S., Wilton, D. C., Apitz-Castro, R., and Jain M. K. (1997). *Biochemistry*, *36*, 12400−21411.
60. Jain, M. K., and Zakim, D. (1987) *Biochim. Biophys. Acta 906*, 33−68.
61. Buckland, A. G., and Wilton, D. C. (2000) *Biochim. Biophys. Acta 1483*, 199−216.
62. Lin, Y., Nielsen, R., Murray, D., Hubbell, W. L., Mailer, C., Robinson, B. H., and Gelb, M. H. (1998) *Science 279*, 1925−1929.
63. Ghomashchi, F., Lin, Y., Hixon, M. S., Yu, B. Z., Amand, R., Jain, M. K.., and Gelb, M. H. (1998) *Biochemistry 37*, 6697−6710.
64. Koduri, R. S., Baker, S. F., Snitko, Y., Han, S. K., Cho, W., Wilton, D. C., and Gelb, M. H. (1998). *J. Biol. Chem. 273*, 32142−32153.
65. Lin, Y., Ghomaschchi, F., Nielson, R., Snitko, Y., Yu, B. Z., S. K., Cho, W., Wilton, D. C., Jain, M. K., Robinson, B. H., and Gelb, M. H. (1998) *Biochem. Soc. Trans.* (U. K.) *26*, 341−345.
66. Yu, B. Z., Janssen, M. J. W., Verheij, H. M., and Jain, M. K. (2000) *Biochemistry*, *39*, 5702−5711.

BI000740K